NANO LETTERS

Letter

pubs.acs.org/NanoLett

Kapitza Resistance between Few-Layer Graphene and Water: Liquid Layering Effects

Dmitry Alexeev,[†] Jie Chen,[†,‡,§] Jens H. Walther,[†,∥] Konstantinos P. Giapis,[⊥] Panagiotis Angelikopoulos,[†] and Petros Koumoutsakos*[,†]

[†]Computational Science and Engineering Laboratory, Department of Mechanical and Process Engineering, ETH Zurich, CH-8092 Zurich, Switzerland

[‡]Center for Phononics and Thermal Energy Science, School of Physics Science and Engineering and [§]Institute for Advanced Study, Tongji University, Shanghai 200092, China

[∥]Department of Mechanical Engineering, Technical University of Denmark, DK-2800 Kgs. Lyngby, Denmark

[⊥]Division of Chemistry and Chemical Engineering, California Institute of Technology, Pasadena, California 91125, United States

Supporting Information

ABSTRACT: The Kapitza resistance (R_K) between few-layer graphene (FLG) and water was studied using molecular dynamics simulations. The R_K was found to depend on the number of the layers in the FLG though, surprisingly, *not* on the water block thickness. This distinct size dependence is attributed to the large difference in the phonon mean free path between the FLG and water. Remarkably, R_K is strongly dependent on the layering of water adjacent to the FLG, exhibiting an inverse proportionality relationship to the peak density of the first water layer, which is consistent with better acoustic phonon matching between FLG and water. These findings suggest novel ways to engineer the thermal transport properties of solid−liquid interfaces by controlling and regulating the liquid layering at the interface.

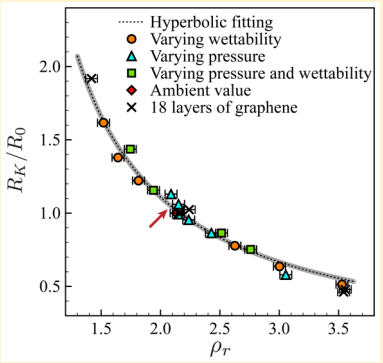

KEYWORDS: *Liquid layering, solid−liquid interface, Kapitza resistance, few-layer graphene, molecular dynamics simulation*

The continuous reduction of dimensions in microelectronic devices has raised serious challenges for their thermal management.[1] Several studies[2−5] have indicated that graphene[6] is a promising material for improved heat dissipation in integrated chips due to its high thermal conductivity. Of particular interest are suspensions of nanoscale graphene flakes and carbon nanotubes in liquids as they exhibit substantially larger thermal conductivity than that of pure liquids.[7] However, there is a discrepancy of more than an order of magnitude between the theoretically predicted and the measured thermal conductivity of nanofluids.[8] This discrepancy is attributed[8] to uncertainties on the value of the interfacial thermal (Kapitza) resistance.

Two models are widely used to describe the interfacial thermal resistance: the acoustic (perfectly specular scattering) and the diffusive mismatch (diffusive scattering) of phonons.[9,10] Both models ignore atomistic details such as the roughness of the interfaces.[10] Molecular dynamics (MD) simulations allow for an atomistic description of the interfaces, and they have been broadly used[11−15] to study their thermal properties.

In this Letter, we examine the Kapitza resistance between few layer graphene (FLG) and water by using nonequilibrium molecular dynamics (NEMD) simulations. We find that the Kapitza resistance depends strongly on the number of graphene layers, while, in contrast, the water thickness has a negligible effect. Remarkably, density layering of the water adjacent to the interface is shown to be the key factor that regulates the Kapitza resistance.

The simulation domain consists of three blocks of FLG separated by two blocks of water (Figure 1), with periodic boundary conditions applied in all directions. Simulations are performed with the LAMMPS package,[16] with a time step of 0.2 fs. Intralayer carbon interactions are modeled with the optimized Tersoff potential,[17] and interlayer carbon interactions are modeled by the pairwise Lennard−Jones (LJ) potential $V(r) = 4\epsilon[(\sigma/r)^{12} - (\sigma/r)^6]$ with parameters taken from ref 18. The graphene−water interactions, essential to this study, are modeled by LJ potential with parameters from ref 19. These potentials have been validated on experimental results, and their uncertainties have been recently quantified.[20] The cutoff distance in LJ potential is set to 2.5σ. Water has been modeled by the flexible simple point-charge (SPC) model[21] and by the rigid SPC water model.[22] Long-range electrostatic forces are computed with the P^3 M method.[23] We note that water and graphene are polar molecules so the effects of polarization might be relevant. However, a recent study by Ho

Received: April 28, 2015

DOI: 10.1021/acs.nanolett.5b03024
Nano Lett. XXXX, XXX, XXX−XXX

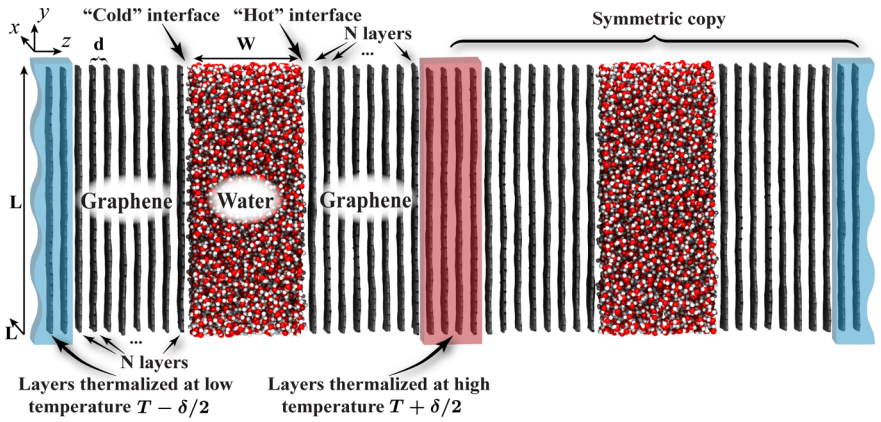

Figure 1. Schematic graph for the simulation setup. Graphene sheets (in black) have size $L \times L$, and the spacing between them is d. Water block (red/white molecules) has the size $L \times L \times W$. Graphene and water blocks are placed one after another along the Z axis. A Nosé−Hoover thermostat at high temperature $T + \delta/2$ (light red region) is applied to four graphene layers in the middle. Another Nosé−Hoover thermostat at low temperature $T - \delta/2$ (light blue region) is applied to the leftmost and rightmost two layers. N nonthermalized layers (black on white background) are situated between water and heat source or sink. Periodic boundary conditions are applied in all directions.

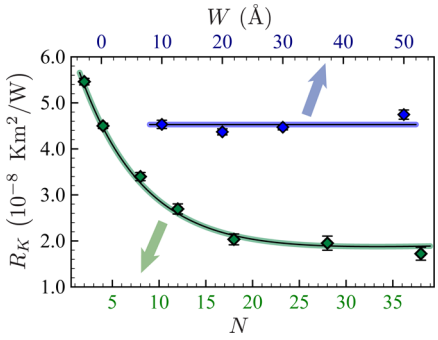

Figure 2. Dependence of Kapitza resistance at graphene−water interface on the size of the solid and the liquid block. N (bottom axis) denotes the number of graphene layers, while W (top axis) denotes the thickness of the water block. Solid lines are drawn to guide the eye. For variable N, the resistance is computed with W = 30 Å, while N = 4 for variable W.

et al.[24] found that polarization of water and graphene has negligible impact on the dynamical properties of graphene−water interface. Further simulation details can be found in the Supporting Information (SI).

NEMD simulations in the NVT ensemble are used to compute the Kapitza resistance,[25] after relaxation of the structure in the NPT ensemble. Nosé−Hoover thermostats[26] are applied to the central and the two ends of the computational domain (Figure 1), respectively. The Kapitza resistance R_K is computed as

$$R_K = \frac{\Delta T}{J} \tag{1}$$

where ΔT is the temperature jump and J is the heat flux across the liquid−solid interface. The temperature jump is computed by a linear regression of the temperature profile, while the heat flux is computed as half of the energy injected into/extracted from the heat source/sink per unit time across unit area (see SI for details). The NEMD simulations are performed sufficiently long (over 5 ns) to ensure a constant heat flux and temperature profile across the system.

The current simulation setup allows us to calculate R_K at two interfaces ("cold" and "hot") with different temperatures (Figure 1). We set the temperature of the thermostat as $T_0 + \delta/2$ and $T_0 - \delta/2$, where T_0 = 300 K is the ambient temperature. In all simulations with various δ, we find that the "cold" interface has consistently larger R_K than the "hot" (see Figure S1c in SI). This result is in agreement with the previous experimental and theoretical studies[9,27] on solid−liquid interfaces. We note that this result is in contrast with previous MD simulations of monatomic liquid−solid interface where a lower Kapitza resistance was associated with the "cold" interface.[11,15] At the same time the present result is consistent with a previous study[28] of the Kapitza resistance at a silicon−water interface.

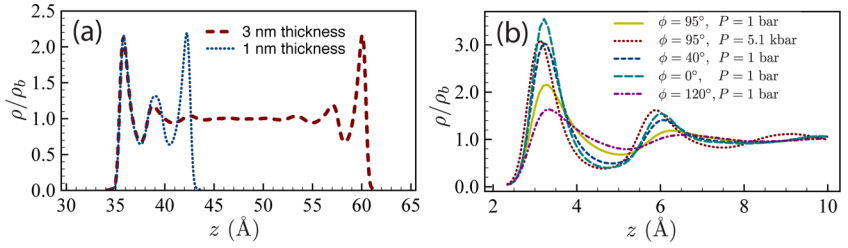

Figure 3. Water density profile adjacent to the graphene−water interface. Here N = 8 is used for all simulations. ρ_b is the bulk-like water density far away from the interface. (a) Different water block thickness at ambient condition (P = 1 bar, ϕ = 95°). The same ρ_b is used for both cases. (b) Reduced water density for different contact angle and pressure. The thickness of the water block is fixed at W = 30 Å for these simulations. For each parameter set, the reference density ρ_b is obtained from the bulk water region without density fluctuation, which is about 1 nm away from the interface.

DOI: 10.1021/acs.nanolett.5b03024
Nano Lett. XXXX, XXX, XXX−XXX

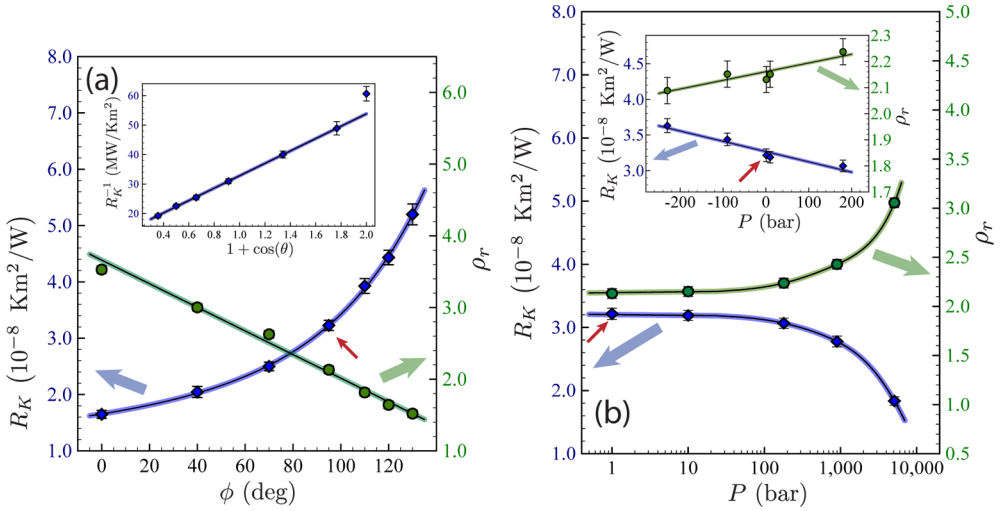

Figure 4. Effect of cross-plane pressure and graphene hydrophobicity on the Kapitza resistance R_K. Here W = 30 Å and N = 8 are used. Solid lines are drawn to guide the eye. Contact angle ϕ (a) and pressure P (b) affect the height of the first density peak of water, which governs interfacial resistance R_K. Blue diamonds represent resistance (left Y-axis), and green circles represent water density (right Y-axis). Thin arrows show ambient case (ϕ = 95°, P = 1 bar) on each plot, and thick arrows point to the corresponding axis. The inset in (a) shows the inverse of Kapitza resistance versus 1 + cos(θ), where θ is the water contact angle.

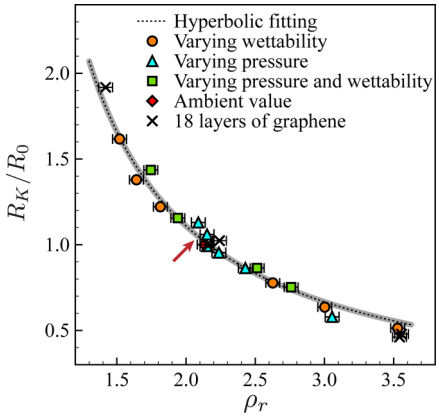

Figure 5. Dependence of normalized interfacial thermal resistance R_K/R_0 on the reduced water density peak ρ_r. Here R_0 is the ambient Kapitza resistance between water and FLG with given number of layers. Hyperbolic fit is shown as a shaded dashed line. Red arrow shows the ambient case (ϕ = 95°, P = 1 bar).

Following ref 11, we report in this study the averaged R_K of the two interfaces. The value of δ does not affect significantly the averaged R_K (see SI), and we set δ = 100 K in our simulations. We also note that the difference in R_K as computed with the flexible and the rigid water models is less than 4% and within the standard deviation of the predictions (see SI). Hereafter we report results using the flexible SPC water model.

We first examine the system size effects on the predictions of R_K. We find that R_K is independent of the cross-sectional area ($L \times L$) when L > 4 nm (see SI). Therefore, we use L = 6 nm and study the dependence of R_K on the thickness of the solid and liquid blocks, separately. With the increase of the number of graphene layers (N), R_K monotonically decreases to an asymptotic value of 2×10^{-8} K m^2/W (Figure 2). A similar size effect has been reported for the Kapitza resistance at solid−solid interfaces.[13,29,30] Based on the acoustic mismatch model, Liang et al.[29] derived an analytical expression of the energy transmission coefficient at a solid−solid interface. They showed that the transmission coefficient depends explicitly on the thickness of the solid and is reduced when the thickness is smaller than the phonon mean free path due to specular reflection at the surface. Previous MD simulations[25,31] suggest that the phonon mean free path in the c-axis of FLG might be greater than 40 layers. Recent experimental measurement of graphite cross-plane thermal conductivity based on a differential 3ω method reports a long phonon mean free path (~200 nm) in the c-axis at room temperature.[32] We postulate that the large phonon mean free path in the solid block is responsible for the size-dependent Kapitza resistance at the graphene−water interface.

In contrast, the thickness of the water block has a negligible effect on R_K (Figure 2), even down to a thickness of 1 nm. This is consistent with the fact that liquids have a much smaller phonon mean free path. In turn, this suggests that only the liquid portion next to the interface affects the interfacial thermal transport. To test this hypothesis, we examine the arrangement of the water molecules adjacent to the graphene−water interface. In contrast to their orientation in bulk water, the water molecules close to the graphene are arranged with their dipole normal to the interface.[33,34] This is indicated by the density profile of water near the interface (Figure 3a) which exhibits strong oscillations.[35,36] Water molecules form "layers" of high density in the proximity of the graphene sheet. The layers are less notable further from the interface, and at a distance of about 0.8−1.0 nm, the water density converges to the bulk value ($\rho_b \approx 1.0$ g/cm^3). Therefore, water undergoes a transition from a distinct orientation in the proximity of graphene to its bulk state away from the interface. We note that for an ultrathin water block of 1 nm, there is no region with constant density of bulk water (Figure 3a). Interestingly, the density layering in the ultrathin water block almost coincides with that in a 3 nm thick water block. Together with the observed negligible size effect of the water block on R_K, this indicates that the density layering of the liquid is critical in determining the interfacial thermal resistance.

To examine how the Kapitza resistance depends on the properties of the liquid layer adjacent to the graphene, we employ two different approaches to modify the interfacial water

DOI: 10.1021/acs.nanolett.5b03024
Nano Lett. XXXX, XXX, XXX−XXX

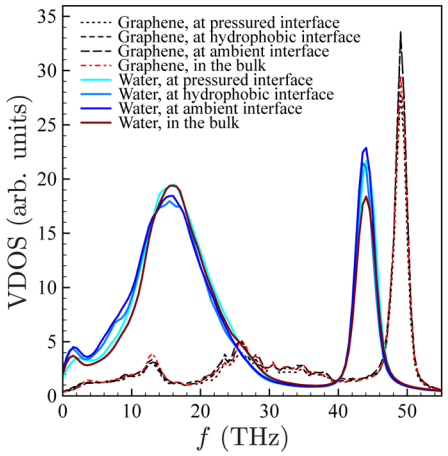

Interface	R_k	Overlap
Ambient	3.228×10^{-8}	0.00270
Pressured	1.871×10^{-8}	0.00263
Hydrophobic	5.198×10^{-8}	0.00271

Figure 6. Left: vibrational density of states (VDOS) of graphene and water. Graphene VDOS at the interface is collected for the outermost layer of graphene. Water VDOS at the interface is collected for water molecules within 0.5 nm from the density peak. VDOS in the bulk was collected in the middle of the corresponding block. Ambient interface: L = 60 Å, W = 30 Å, T = 300 K, δ = 100 K, P = 1 bar, ϕ = 95°; pressured interface: L = 60 Å, W = 30 Å, T = 300 K, δ = 100 K, P = 5.1 kbar, ϕ = 95°; hydrophobic interface: L = 60 Å, W = 30 Å, T = 300 K, δ = 100 K, P = 1 bar, ϕ = 130°. Right: overlap in VDOS spectra of graphene and water for different interfaces. Clearly the resistance difference is not attributed to the overlap.

properties. First, we tune the graphene hydrophobicity by varying ϵ with fixed σ for the LJ potential acting between the oxygen and carbon atoms. It has been shown[19] that there is a linear dependence between the energy parameter (ϵ) and the contact angle of a water droplet on a graphene sheet. As shown in Figure 3b, the peak value of the water density layering is larger next to the hydrophilic interface, while the water density away from the interface is independent of its wettability. To quantify the water density difference, we define the reduced water density peak $\rho_r = \rho_{max}/\rho_b$, where ρ_{max} is the first water density peak close to graphene and ρ_b is the bulk-like water density far away from the interface. By computing R_K at different water contact angle, we find that the graphene hydrophobicity has significant impact on the Kapitza resistance (Figure 4(a)), consistent with previous studies.[11,15,37] We find that R_K varies from ∼1.6 × 10^{-8} K m^2/W for a strongly hydrophilic interface (contact angle is 0°) to ∼5.2 × 10^{-8} K m^2/W for a strongly hydrophobic interface (contact angle is 130°). Moreover, Shenogina et al.[37] found the interfacial thermal conductance between water/self-assembled monolayers is proportional to the work of adhesion. We observe the same dependence for graphene−water interface in our study (see the inset of Figure 4a), suggesting that the functional dependence of the interfacial thermal conductance on the work of adhesion is general across different types of interfaces. More importantly, we find that the Kapitza resistance correlates well with the density layering of the water: the higher the water density peak (ρ_r), the lower the interfacial thermal resistance.

To verify this correlation, we modify the water density by applying an external pressure field in the direction perpendicular to the interface.[25] We find that the Kapitza resistance and density peak of water are both affected by the external pressure, while the same correlation holds between Kapitza resistance and water density peak (Figure 4b). Increased compressive pressure lowers R_K, while tensile pressure results in higher R_K. The maximum pressure applied in our simulations is 5100 bar for the compressive case and 230 bar for the tensile case. In both cases induced strain of FLG appears to be small, so that phonon density of states remains practically unchanged.[25] The density of the whole water block increases with increasing compressive pressure, but a larger change occurs in the first water density peak next to the graphene sheet (Figure 3b). For compressive pressure of 900 bar the change in ρ_b and ρ_{max} are, respectively, ∼ 4% and ∼16%. The resultant water density profiles show striking similarity to those obtained by varying the graphene hydrophobicity. The first water density peak, located at about 3.2 Å from the graphene is highly pronounced and followed by several smaller peaks (Figure 3b). Bulk water density is reached beyond 8−10 Å away from the graphene. Similar results are observed when we vary simultaneously the system pressure and the graphene hydrophobicity. These results imply that the first density peak of water adjacent to the interface is the critical factor that determines the value of the Kapitza resistance and independent of the method by which it is induced (Figure 5). We note that the dependence of the Kapitza resistance to the increased density of the liquid at the interface was first noted by Challis et al.[38] in experiments with liquid helium and various solids. They noted that the phonon transmission was enhanced due to this compressed layer of liquid adjacent to the solid.[38,39]

Moreover, we have performed a number of simulations (ambient condition, P = 5100 bar, P = 180 bar, ϕ = 0°, ϕ = 130°) with 18 layers of graphene. Figure 5 summarizes the results of all simulations for the rescaled Kapitza resistance (R_K/R_0) where R_0 is the Kapitza resistance at ambient conditions. We observe a consistent decrease of R_K/R_0 with ρ_r. Following the classical theory for the inverse dependence of the Kapitza resistance on liquid density,[9] we fit all of the simulation data with the following function:

$$\frac{R_K}{R_0} = \frac{A}{\rho_r + B} \tag{2}$$

Setting A = 1.67 and B = −0.49, the correlation factor for the fit is 0.975, and the standard deviations of both values ∼5%. Remarkably, we find that all results from our simulations collapse on this curve that shows the inverse dependence of Kapitza resistance on the first density peak of the liquid. Both the liquid density and temperature dependencies (see SI) suggest that the acoustic mismatch model may capture better the essential process of phonon propagation across the graphene−water interface.

DOI: 10.1021/acs.nanolett.5b03024
Nano Lett. XXXX, XXX, XXX−XXX

To better understand the mechanism of the Kapitza resistance dependence on the water density peak, we have calculated the vibrational density of states (VDOS) of graphene and water adjacent to the interface (Figure 6). We observe insignificant spectrum change for interfaces with highly dissimilar R_K. Moreover, we have calculated an overlap S of VDOS of graphene and water (for details, see ref 40):

$$S = \frac{\int_0^\infty P_G(f)P_W(f)\mathrm{d}f}{\int_0^\infty P_G(f)\mathrm{d}f \int_0^\infty P_W(f)\mathrm{d}f} \quad (3)$$

The yielded overlaps (Figure 6, right) differ in less than 3%, while the Kapitza resistance undergoes almost 3-fold difference. Therefore, we conclude that change in R_K does not originate from the change in VDOS. Combining this result with the dependence in Figure 5, we can further conclude that the heat transfer is promoted (or suppressed) at the solid−liquid interface mainly because of the aggregation of more (accordingly, less) water molecules at the interface. This finding is distinct to the case of solid−solid interface, where the density change at each side is negligible and the heat transfer is regulated by the overlap of phonon spectrum.[40]

In summary, we investigated the thermal transport across water−graphene interface through NEMD simulations. The Kapitza resistance depends on the thickness of the FLG, though, surprisingly, it is independent of the water block thickness. This dissimilar dependence is attributed to the large differences in the phonon mean free path in FLG and water. On the other hand, the Kapitza resistance is critically affected by the water layering at the interface and more specifically by the value of the first density peak of water adjacent to the interface. By imposing global cross-plane pressure and by changing graphene hydrophobicity, we were able to change the water density peak and, it turn, to tune the Kapitza resistance. The magnitude of the first density peak of a liquid adjacent to the solid may be tuned to control the heat dissipation in micro- and nanofluidic systems.

■ ASSOCIATED CONTENT

Supporting Information

The Supporting Information is available free of charge on the ACS Publications website at DOI: 10.1021/acs.nanolett.5b03024.

Simulation procedures and characterization data (PDF)

■ AUTHOR INFORMATION

Corresponding Author

*E-mail: petros@ethz.ch.

Author Contributions

D.A. and J.C. contributed equally to this work.

Notes

The authors declare no competing financial interest.

■ ACKNOWLEDGMENTS

J.C. acknowledges support as an ETH Zurich Fellow and the EU Marie Curie Actions for People COFUND Program, the startup grant (No. 152225) at Tongji University, and the National Youth 1000 Talents Program in China. P.A. and P.K. acknowledge support by the European Research Council (Advanced Investigator Award No. 2-73985-14).

■ REFERENCES

(1) Moore, A. L.; Shi, L. *Mater. Today* **2014**, *17*, 163−174.
(2) Balandin, A. A.; Ghosh, S.; Bao, W.; Calizo, I.; Teweldebrhan, D.; Miao, F.; Lau, C. N. *Nano Lett.* **2008**, *8*, 902−907.
(3) Balandin, A. A. *Nat. Mater.* **2011**, *10*, 569−581.
(4) Cai, W. W.; Moore, A. L.; Zhu, Y. W.; Li, X. S.; Chen, S. S.; Shi, L.; Ruoff, R. S. *Nano Lett.* **2010**, *10*, 1645−1651.
(5) Chen, S.; Wu, Q.; Mishra, C.; Kang, J.; Zhang, H.; Cho, K.; Cai, W.; Balandin, A.; Ruoff, R. *Nat. Mater.* **2012**, *11*, 203−207.
(6) Novoselov, K. S.; Geim, A. K.; Morozov, S. V.; Jiang, D.; Zhang, Y.; Dubonos, S. V.; Grigorieva, I. V.; Firsov, A. A. *Science* **2004**, *306*, 666−669.
(7) Wang, X. Q.; Mujumdar, A. S. *Int. J. Therm. Sci.* **2007**, *46*, 1−19.
(8) Huxtable, S. T.; Cahill, D. G.; Shenogin, S.; Xue, L.; Ozisik, R.; Barone, P.; Usrey, M.; Strano, M. S.; Siddons, G.; Shim, M.; Keblinski, P. *Nat. Mater.* **2003**, *2*, 731−734.
(9) Pollack, G. L. *Rev. Mod. Phys.* **1969**, *41*, 48−81.
(10) Swartz, E. T.; Pohl, R. O. *Rev. Mod. Phys.* **1989**, *61*, 605−668.
(11) Barrat, J.-L.; Chiaruttini, F. *Mol. Phys.* **2003**, *101*, 1605−1610.
(12) Konatham, D.; Striolo, A. *Appl. Phys. Lett.* **2009**, *95*, 163105.
(13) Landry, E. S.; McGaughey, A. J. H. *Phys. Rev. B: Condens. Matter Mater. Phys.* **2009**, *80*, 165304.
(14) Chen, J.; Zhang, G.; Li, B. *J. Appl. Phys.* **2012**, *112*, 064319.
(15) Kim, B. H.; Beskok, A.; Cagin, T. *J. Chem. Phys.* **2008**, *129*, 174701.
(16) Plimpton, S. *J. Comput. Phys.* **1995**, *117*, 1−19.
(17) Lindsay, L.; Broido, D. A. *Phys. Rev. B: Condens. Matter Mater. Phys.* **2010**, *81*, 205441.
(18) Girifalco, L. A.; Hodak, M.; Lee, R. S. *Phys. Rev. B: Condens. Matter Mater. Phys.* **2000**, *62*, 13104−13110.
(19) Werder, T.; Walther, J. H.; Jaffe, R. L.; Halicioglu, T.; Koumoutsakos, P. *J. Phys. Chem. B* **2003**, *107*, 1345−1352.
(20) Angelikopoulos, P.; Papadimitriou, C.; Koumoutsakos, P. *J. Chem. Phys.* **2012**, *137*, 144103.
(21) Wu, Y.; Tepper, H. L.; Voth, G. A. *J. Chem. Phys.* **2006**, *124*, 024503.
(22) Berendsen, H. J. C.; Grigera, J. R.; Straatsma, T. P. *J. Phys. Chem.* **1987**, *91*, 6269−6271.
(23) Hockney, R. W.; Eastwood, J. W. *SIAM Reviews*; CRC Press; Boca Raton, FL, 1988.
(24) Ho, T. A.; Striolo, A. *J. Chem. Phys.* **2013**, *138*, 054117.
(25) Chen, J.; Walther, J. H.; Koumoutsakos, P. *Nano Lett.* **2014**, *14*, 819−825.
(26) Martyna, G. J.; Klein, M. L. *Phys. Rev. Lett.* **1992**, *97*, 2635.
(27) Stoner, R. J.; Maris, H. J. *Phys. Rev. B: Condens. Matter Mater. Phys.* **1993**, *48*, 16373−16387.
(28) Murad, S.; Puri, I. K. *Appl. Phys. Lett.* **2008**, *92*, 133105.
(29) Liang, Z.; Sasikumar, K.; Keblinski, P. *Phys. Rev. Lett.* **2014**, *113*, 1−5.
(30) Chang, S.-W.; Nair, A. K.; Buehler, M. J. *J. Phys.: Condens. Matter* **2012**, *24*, 245301.
(31) Wei, Z.; Ni, Z.; Bi, K.; Chen, M.; Chen, Y. *Phys. Lett. A* **2011**, *375*, 1195−1199.
(32) Fu, Q.; Yang, J.; Chen, Y.; Li, D.; Xu, D. *Appl. Phys. Lett.* **2015**, *106*, 031905.
(33) Walther, J. H.; Jaffe, R.; Halicioglu, T.; Koumoutsakos, P. *J. Phys. Chem. B* **2001**, *105*, 9980−9987.
(34) Jaffe, R. L.; Gonnet, P.; Werder, T.; Walther, J. H.; Koumoutsakos, P. *Mol. Simul.* **2004**, *30*, 205−216.
(35) Gao, J.; Luedtke, W.; Landman, U. *Phys. Rev. Lett.* **1997**, *79*, 705−708.
(36) Cicero, G.; Grossman, J. C.; Schwegler, E.; Gygi, F.; Galli, G. *J. Am. Chem. Soc.* **2008**, *130*, 1871−1878.
(37) Shenogina, N.; Godawat, R.; Keblinski, P.; Garde, S. *Phys. Rev. Lett.* **2009**, *102*, 156101.
(38) Challis, L. J.; Dransfeld, K.; Wilks, J. *Proc. R. Soc. London, Ser. A* **1961**, *260*, 31−46.

DOI: 10.1021/acs.nanolett.5b03024
Nano Lett. XXXX, XXX, XXX−XXX

(39) Cahill, D. G.; Ford, W. K.; Goodson, K. E.; Mahan, G. D.; Majumdar, A.; Maris, H. J.; Merlin, R.; Phillpot, S. R. *J. Appl. Phys.* **2003**, *93*, 793−818.
(40) Chen, J.; Zhang, G.; Li, B. *Appl. Phys. Lett.* **2009**, *95*, 073117.

DOI: 10.1021/acs.nanolett.5b03024
Nano Lett. XXXX, XXX, XXX−XXX